NEW FINITE ELEMENT FOR PIEZOELECTRIC MODELING OF PLATES AND SHELLS STRUCTURES

Olivier Polit, Michele d'Ottavio, Philippe Vidal

XI ECCOMAS Thematic Conference on Smart Structures and Materials
SMART 2025
M. Krommer, M. Nader, M. Schagerl and A. Benjeddou (Eds)

NEW FINITE ELEMENT FOR PIEZOELECTRIC MODELING OF PLATES AND SHELLS STRUCTURES

O. Polit, M. D'Ottavio and P. Vidal

LEME - Univ. Paris Nanterre
50 rue de Sèvres
92410 Ville d'Avray - France
e-mail: opolit@parisnanterre.fr

Abstract. This paper presents a C^0 8-node quadrilateral finite element (FE) for geometrically linear piezoelectric plates/shells. It is based on a high-order kinematics proposed in [1] for the mechanical part. Furthermore, Murakami's ZigZag Function [2] is superimposed for the three displacement components for improving the accuracy for multilayered modeling. The approximation of the electric potential must be able to model piezoelectric patches, and a constant value is considered on each elementary domain while a cubic variation in each layer is used, based on the polynomial expansion given in [3]. A plate/shell FE is finally deduced with nine degrees of freedom (dof) per node for the mechanical part, twelve dofs if the ZigZag functions are included [4] and, for the layerwise description of the piezoelectric behavior, three additional dof per element and per layer are added.

This FE is evaluated on two piezoelectric plate/shell tests including sensor and actuator configurations. The role of electrode segmentation, i.e. the size of equipotential surfaces, on the electro-mechanical response has been also considered.

Key words: Composite structures, finite element, high-order model, Zig-Zag function, piezoelectric patch analysis

1 Introduction

Research and development concerning high-performance structures are very intense since some decades. Structural health monitoring, active vibration damping, and energy harvesting are some examples of possible applications of a multifunctional structural component. Piezoelectric materials permit to convert mechanical and electrical energy at frequency ranges that are most interesting for technical applications such as vibration damping and rapid shape adaptation [5]. Development of theoretical and numerical models for this kind of structures is very important and active. For this purpose and in the framework of two-dimensional plate/shell models, different choices can be made for the mechanical approximation and the following classification is classically admitted for the variation in the thickness direction: (i) Equivalent Single Layer (ESL) models, in which the number of unknowns is independent of the layer

number; (ii) Layer-Wise (LW) descriptions, for which the number of unknowns and, thus, the computational cost increases with the number of layers. While most developments employ an ESL description for the mechanical behavior, and particularly the First order Shear Deformation Theory (FSDT), a Layer-Wise description is necessary for the piezoelectric approximation to impose electric boundary conditions at each piezoelectric layer interfaces, i.e., the electrodes, within the stack. Inside each piezoelectric layer, the electric potential can be linear, quadratic or higher and a comparison has been proposed in [6].

A review of different approaches is available in [7, 8] and in the framework of the Carrera Unified Formulation (CUF) in [9]. For the FE approximations, a review limited to shell models is also given in [10].

The limitation of the FSDT model is related to the constant transverse displacement hypothesis, inducing no thickness change and the use of the reduced 2D constitutive law. The use of the full 3D constitutive law is an important feature for a consistent representation of complex physical interactions like multi-field coupling. Furthermore, accurate modelling of thick structures needs the transverse normal stress and the 3D constitutive law.

Therefore, a high-order model is chosen with sinus function for the in-plane displacements and quadratic assumption along the thickness of the transverse deflection. Thus, the 3D constitutive law is retained along with a parabolic distribution of the transverse shear strains and a linear variation of the transverse normal strain are recovered. In order to introduce transverse strain discontinuities required to fulfill the interlaminar equilibrium, Murakami's Zig-Zag function (MZZF) [2] is superimposed to the high-order ESL kinematics for the 3 displacement components. Note that MZZF does not depend on the constitutive coefficients and is, hence, attractively simple in conjunction with three-dimensional constitutive laws including multi-field coupling. Based on this kinematics, an 8-node shell Finite Element (FE) is proposed, free of numerical illness such as transverse shear and Poisson lockings, oscillation and spurious mechanics [1]. The approximation of the electric potential must be able to model piezoelectric patches, and a constant value is considered on each elementary domain while a cubic variation in each layer is used, based on the polynomial expansion proposed in [3, 11].

The paper is organized as follows: Section 2 describes the plate problem, the approximations for the displacement and the electric potential and the system to be solved. The resulting FE is evaluated in Section 3 for composite plate and shell, and electrode segmentation modelling is discussed.

2 Description of the plate problem

2.1 Governing equations

Let us consider a plate occupying the domain $\mathcal{V} = \Omega \times [-\frac{e}{2} \leq z \leq \frac{e}{2}]$ in a Cartesian coordinate system $(x_1, x_2, x_3 = z)$. The plate is defined by an arbitrary surface Ω in the (x_1, x_2) plane, located at the midplane for $z = 0$, and by a constant thickness e.

The primary variables are the displacements vector field $\vec{u}(x_1, x_2, z)$ and the scalar electric potential $\phi(x_1, x_2, z)$. $\varepsilon_{ij}(x_1, x_2, z)$ and $\vec{E}(x_1, x_2, z)$ are the strain tensor components and the elec-

tric field vector, respectively, deduced from primary variables by the geometric relations. Furthermore, $\sigma_{ij}(x_1,x_2,z)$ and $\vec{D}(x_1,x_2,z)$ are the conjugated fluxes (stress tensor components and dielectric displacement vector, respectively) obtained from the constitutive equations given in the next subsection.

2.1.1 Constitutive relation

The 3D constitutive equation for a linear piezoelectric material is given by the following set of coupled equations [12] for a layer (k):

$$[\sigma^{(k)}] = [C^{(k)}]\,[\varepsilon^{(k)}] - [e^{(k)}]^T\,[E^{(k)}] \tag{1a}$$

$$[D^{(k)}] = [e^{(k)}]\,[\varepsilon^{(k)}] + [\varepsilon^{(k)}]\,[E^{(k)}] \tag{1b}$$

where we denote by $[C]$ the matrix of elastic stiffness coefficients taken at constant electric field, by $[e]$ the matrix of piezoelectric stress coefficients and by $[\varepsilon]$ the matrix of electric permittivity coefficients taken at constant strain. The explicit form of these matrices can be found in [10] for an orthotropic piezoelectric layer polarized along the thickness direction z. Eq. (1a) expresses the piezoelectric *converse* effect for actuator applications, whereas Eq. (1b) represents the piezoelectric *direct* effect which is exploited in sensor applications. Note that the constitutive law is expressed in the local reference frame associated to each layer.

2.1.2 The weak form of the boundary value problem

The classical piezoelectric variational formulation of [13] is employed in which the primary field variables are the "generalized displacements", i.e. the displacement field, and the electrostatic potential. Using a matrix notation and for admissible virtual displacements $\vec{u}^*$ and electric potential ϕ^* (virtual quantities are denoted by an asterisk), the variational principle is given by:

$$\begin{aligned}\int_{\mathcal{V}} \rho [u^*]^T [\ddot{u}]\, d\mathcal{V} = &- \int_{\mathcal{V}} [\varepsilon(u^*)]^T [\sigma(u,\phi)]\, d\mathcal{V} + \int_{\mathcal{V}} [u^*]^T [f]\, d\mathcal{V} + \int_{\partial\mathcal{V}_F} [u^*]^T [F]\, d\partial\mathcal{V} \\ &+ \int_{\mathcal{V}} [E(\phi^*)]^T [D(u,\phi)]\, d\mathcal{V} - \int_{\mathcal{V}} q\,\phi^*\, d\mathcal{V} - \int_{\partial\mathcal{V}_Q} Q\,\phi^*\, d\partial\mathcal{V}\end{aligned} \tag{2}$$

where $[f]$ is the body force vector, $[F]$ the surface force vector applied at $\partial\mathcal{V}_F$, q the volume charge density, Q the surface charge density supplied on $\partial\mathcal{V}_Q$ and ρ is the mass density. Finally, $\varepsilon(u^*)$ and $E(\phi^*)$ are the virtual strain and virtual electric field that satisfy the compatibility gradient equations. In the remainder of this article we will refer only to static problems, for which the left-hand side term is set to zero. Furthermore, body forces and volume charge densities will be discarded ($[f] = [0]$; $q = 0$).

2.2 The mechanical part

2.2.1 The displacement field

Based on the sinus model, see [14], a new plate model which takes into account the transverse normal stress is presented in this section. This extension is based on following developments

- various models for beams, plates and shells based on the refined sinus theory, see [14, 15, 16, 17, 18, 19];
- our previous paper on a 7 parameter model for thermo-mechanical analysis [1].

In the framework of ESL approach, the kinematics of our model is assumed to have the following particular form

$$\left\{\begin{array}{lcl} U_1(x_\alpha,z) &=& {u^0}_1(x_\alpha)+z\,{u^1}_1(x_\alpha)+f(z)\,{u^f}_1(x_\alpha) \\ U_2(x_\alpha,z) &=& {u^0}_2(x_\alpha)+z\,{u^1}_2(x_\alpha)+f(z)\,{u^f}_2(x_\alpha) \\ U_3(x_\alpha,z) &=& {u^0}_3(x_\alpha)+z\,{u^1}_3(x_\alpha)+z^2\,{u^2}_3(x_\alpha) \end{array}\right. \tag{3}$$

where $\alpha \in \{1,2\}$ and $i \in \{1,2,3\}$. In Eq. (3), the superscript is associated to the expansion order in z while the subscript is related to the component of the displacement. Thus, ${u^0}_i$ are the displacements of a point of the reference surface, while $({u^1}_\alpha, {u^f}_\alpha)$ measure the rotations about the axis $(0,x_\alpha)$ and the warping of the normal transverse fiber, respectively. The functions ${u^\alpha}_3$ permit to have a non-constant deflection for the transverse fiber and allow to have non zero transverse normal stretch. Furthermore, the quadratic assumption for the transverse displacement avoids the occurrence of Poisson (or thickness) locking, see [1].

In the context of the sinus model, we have

$$f(z) = \frac{e}{\pi}\sin\frac{\pi z}{e} \tag{4}$$

It must be noticed that the classical homogeneous sinus model [14] can be recovered from Eq. (3) assuming ${u^1}_\alpha = -{u^0}_{3,\alpha}$, and discarding the unknown functions ${u^\alpha}_3$.

2.2.2 The Murakami's Zig-Zag terms

In order to evaluate the influence of Zig-Zag terms [2] in a high-order ESL model, the following contributions per layer (k) could be added to Eq. (3):

$$\left\{\begin{array}{lcl} {U_1}^{(k)}(x_\alpha,z) &=& Z^{(k)}(z)\,{u^z}_1(x_\alpha) \\ {U_2}^{(k)}(x_\alpha,z) &=& Z^{(k)}(z)\,{u^z}_2(x_\alpha) \\ {U_3}^{(k)}(x_\alpha,z) &=& Z^{(k)}(z)\,{u^z}_3(x_\alpha) \end{array}\right. \tag{5}$$

with

$$Z^{(k)}(z) = (-1)^k\,\zeta_k(z) \quad \text{and} \quad \zeta_k(z) = \frac{2}{e_k}\left(z - \frac{1}{2}(z_k + z_{k+1})\right) \tag{6}$$

where e_k is the thickness of the k^{th} layer while (z_k, z_{k+1}) are the bottom and top coordinates of this layer. It is obvious that $Z^{(k)}(z)$ is a piecewise linear function with bi-unit amplitude for all the layers as we have $\zeta_k(z) \in [-1,1]$. Note that, despite the $Z^{(k)}(z)$ function depends on the layer index inside the stack, the amplitudes $u^z{}_i$ are unique for the whole laminate, i.e., the ESL framework is still preserved.

2.3 The electric part

On each elementary domain Ω_e, the electric potential is assumed to be constant. Therefore, no variation with respect to x_α is considered. A cubic layerwise (LW) description is used across the thickness, according to the approximation introduced in [3] and used in [11]: in each layer (k), the electric potential distribution is described by the normal electric field components at the bottom and top surfaces, denoted E_{3b} and E_{3t}, respectively, and the potential difference $\Delta\phi$ between top and bottom surface. Using these dofs, the approximation of the electric potential can be written as:

$$\left[\phi^{(k)}\right] = \left[F_\phi\right] \left[Cst_\phi^{(k)}\right] \left[q_\phi^{e(k)}\right] \tag{7}$$

where the following definitions have been introduced:

$$\left[F_\phi\right] = \left[\begin{array}{cccc} 1 & z & z^2 & z^3 \end{array}\right]; \quad \left[q_\phi^{e(k)}\right]^T = \left[\begin{array}{ccc} E_{3b}{}^{(k)} & \Delta\phi^{(k)} & E_{3t}{}^{(k)} \end{array}\right] \tag{8}$$

and $\left[Cst_\phi{}^{(k)}\right]$ is a (4×3) matrix containing constant coefficients. The electric field vector in each layer $\left[E^{(k)}\right]$ is then obtained as:

$$\left[E^{(k)}\right] = \left[\begin{array}{c} 0 \\ 0 \\ -\phi_{,3}^{(k)} \end{array}\right] = [F_E] \left[Cst_E{}^{(k)}\right] \left[q_\phi{}^{e(k)}\right] \text{ with } [F_E] = \left[\begin{array}{ccc} 1 & z & z^2 \end{array}\right] \tag{9}$$

where $\left[Cst_E{}^{(k)}\right]$ is a (3×3) matrix. So, the adopted approximation yields a quadratic transverse electric field across the thickness of each layer.

2.4 The system to be solved

The FE approximations are not detailed here for the sake of brevity and can be found elsewhere [10, 1]. The eight-node quadrilateral finite element is used and classical FE approximation is used for the geometry. A special treatment is used to control the transverse shear locking by using a dedicated interpolation for $\gamma_{\alpha 3}{}^0$ according to the methodology presented in [1]. Note that since the electric potential is assumed to be constant on each elementary domain, there is no need to introduce any FE approximation for this field.

The elementary matrices are then deduced from the bi-dimensional weak form obtained from Eq. (2) upon carrying out the integral along the thickness z. Assembling each elementary

contribution in the global reference frame, the following discrete form of the coupled piezoelectric system is obtained:

$$\begin{bmatrix} [K_{uu}] & [K_{u\phi}] \\ [K_{u\phi}]^T & [K_{\phi\phi}] \end{bmatrix} \begin{bmatrix} [q_u] \\ [q_\phi] \end{bmatrix} = \begin{bmatrix} [L_u] \\ [L_\phi] \end{bmatrix} \tag{10}$$

where $[K_{uu}]$, $[K_{\phi\phi}]$ and $[K_{u\phi}]$ are the global stiffness, dielectric and piezoelectric matrices of the plate, respectively. The mechanical dofs are in the vector $[q_u]$, while the electrical dofs are in the vector $[q_\phi]$ and we have at the elementary level

$$\begin{aligned} [q_u{}^e] &= \left[\begin{pmatrix} u^0{}_1 & u^0{}_2 & u^0{}_3 \,|\, u^1{}_1 & u^1{}_2 & u^1{}_3 \,|\, u^f{}_1 & u^f{}_2 & u^2{}_3 \,|\, u^z{}_1 & u^z{}_2 & u^z{}_3 \end{pmatrix}_{i=1,8}\right] \\ [q_\phi{}^e] &= \left[\begin{pmatrix} E_{3b}{}^{(k)} & \Delta\phi^{(k)} & E_{3t}{}^{(k)} \end{pmatrix}_{k=1,Nl}\right] \end{aligned} \tag{11}$$

with Nl the number of layers. From the mechanical point of view, the Zig-Zag dofs can be activated or not: the P9 model corresponds to the case of no Zig-Zag dof, P9Z denotes the model using only in-plane Zig-Zag dof $u^z{}_\alpha$, and P9ZZ denotes the FE with all the Zig-Zag dof $u^z{}_i$. So, the three models P9, P9Z and P9ZZ use 9, 11 and 12 kinematical unknown functions, respectively, and the associated FE have 72, 88, 96 mechanical dofs per element, respectively.

Since the electric potential is assumed constant on each FE, the assembly involves only the approximation along the thickness. A piezoelectric patch comprising several FEs can be defined through the imposition of the equipotential condition between electrodes: the same $\Delta\phi$ is imposed on the piezoelectric layer for all elements belonging to the same patch. From the numerical point of view, this is accomplished through linear homogeneous and non-homogeneous Multi-Point Constraints (MPC) using penalty function method.

In Eq. (10), the load vectors $[L_u]$ and $[L_\phi]$ represent the external loading from applied forces and prescribed charges, respectively. Essential boundary conditions (i.e., prescribed displacements and electric potentials) are imposed numerically by a penalty technique. The coupled system is then solved by the classical static condensation procedure for the electrical dof:

$$[q_\phi] = [K_{\phi\phi}]^{-1}([L_\phi] - [K_{u\phi}]^T [q_u]) \tag{12a}$$

which yields the following purely mechanical system with a modified equivalent stiffness matrix:

$$\left[[K_{uu}] - [K_{u\phi}][K_{\phi\phi}]^{-1}[K_{u\phi}]^T\right][q_u] = [L_u] - [K_{u\phi}][K_{\phi\phi}]^{-1}[L_\phi] \tag{12b}$$

In the remainder of the paper, $[L_\phi] = [0]$ will be considered.

3 Numerical results

3.1 Clamped composite plate

This test is interesting to evaluate the segmentation of a piezoelectric layer using different number of patches. It considers first the sensory response of a cantilever, square, hybrid plate

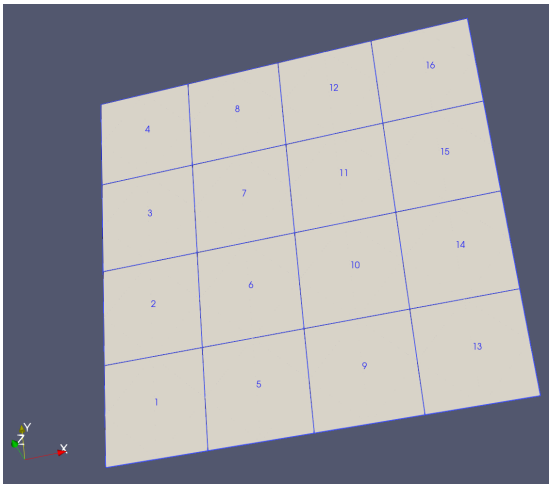

Figure 1: Mesh $N = 4$ and element numbers.

with one edge clamped and other edges free subjected to a uniform pressure load. It has been widely used in the literature [20] and recently re-considered [21] to evaluate the segmentation of the electrode sensor surfaces :

geometry square plate 200×200 mm^2 and total thickness $e = 1.2$ mm,

materials seven-layers $(pz, 45°, -45°, 45°, -45°, pz)$; the outer piezoelectric layers of thickness 0.1 mm are made out of PZT-G1195N material with opposite polarization directions normal to the mid-surface; and four inner layers of graphite/epoxy (T300/976) with thickness $e = 0.25$ mm. The material properties are given in Tab. 1,

boundary conditions clamped at $x_1 = 0$; uniform pressure load p_0; piezoelectric layers can be in sensor configuration ($\Delta\phi$ let free) or in actuator configuration ($\Delta\phi \neq 0$); actuator configuration is considered by imposing $-\Delta\phi$ in the bottom layer and $\Delta\phi$ in the top one,

mesh four regular meshes $N \times N$ are used, with $N \in \{2, 4, 8, 16\}$; Fig. 1 presents the $N = 4$ case.

results and locations transverse displacement at the center tip of the free edge and piezoelectric potential distribution.

Fig. 2 (left) presents the convergence of the transverse displacement of P9 FE, with five values along the central line of the plate, when electric potential load ± 10 V is applied at the bottom and top layer. The convergence is very fast for the transverse displacement and the mesh $N = 4$ will be used for the following simulations. The actuator effect is presented in Fig. 2 (right) for the shape control of the plate subjected to a uniform pressure load. Increasing the

Prop.	PZT -G1195N	T300 /976	PZT4	Graphite -epoxy	Prop.	PZT -G1195N	T300 /976	PZT4	Graphite -epoxy
E_1 [GPa]	63.0	150.0	81.3	132.4	e_{15} [C/m^2]			12.72	
E_2 [GPa]	63.0	9.0	81.3	10.8	e_{24} [C/m^2]			12.72	
E_3 [GPa]	63.0	9.0	64.5	10.8	e_{31} [C/m^2]	30.8		-5.2	
ν_{23}	0.30	0.3	0.43	0.49	e_{32} [C/m^2]	30.8		-5.2	
ν_{13}	0.30	0.3	0.43	0.24	e_{33} [C/m^2]	18.5		15.08	
ν_{12}	0.30	0.3	0.33	0.24	ε_{11} [nF]	15.3	ε_0	13.05	ε_0
G_{23} [GPa]	24.2	2.5	25.6	3.6	ε_{22} [nF]	15.3	ε_0	13.05	ε_0
G_{13} [GPa]	24.2	7.1	25.6	5.6	ε_{33} [nF]	15.0	ε_0	11.5	ε_0
G_{12} [GPa]	24.2	7.1	30.6	5.6					

Table 1: Material properties used in the plate and shell problems.

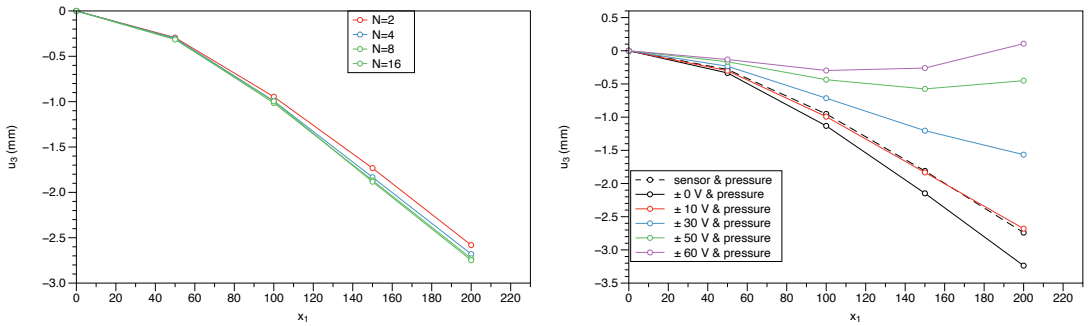

Figure 2: Clamped composite plate: convergence of the transverse displacement along the central line for actuator configuration ($\pm 10V$) (left) and distribution of the transverse displacement under uniform pressure load and variation of the electric potential (right).

voltage of the actuation induces a decrease of the deflection of the plate. When a voltage of ± 60 V is applied, the transverse displacement at the cantilever's tip becomes slightly positive.

The effect of electrode segmentation is evaluated for the open circuit boundary condition. Fig. 3 reports the output (sensed) voltage at the bottom and top $pz-$layers for 4 different electrode configurations represented by a 4×4 FE mesh: (i) 4×4 electrode grid (i.e., one electrode per FE); (ii) 2×2 electrode grid (i.e., 4 patches, each consisting of 4 FE); (iii) 4 strips of electrodes, segmenting the plate along the x_1 axis in 4 patches covering the whole plate's width; (iv) 2 strips of electrodes, segmenting the plate along the x_1 axis in 2 patches covering the whole plate's width. Note that the employed mesh is illustrated in Fig. 1, where the element numbers can be found that are given in the abscissa of the figures. The results are in agreement with expected values and it can be noticed that the high voltage is located close to the clamped side. As expected, the 2×2 grid gives symmetric results with the same values of the 2 strip grid configuration, as there are no gradients in the (O, x_2) direction. The maximum voltage output

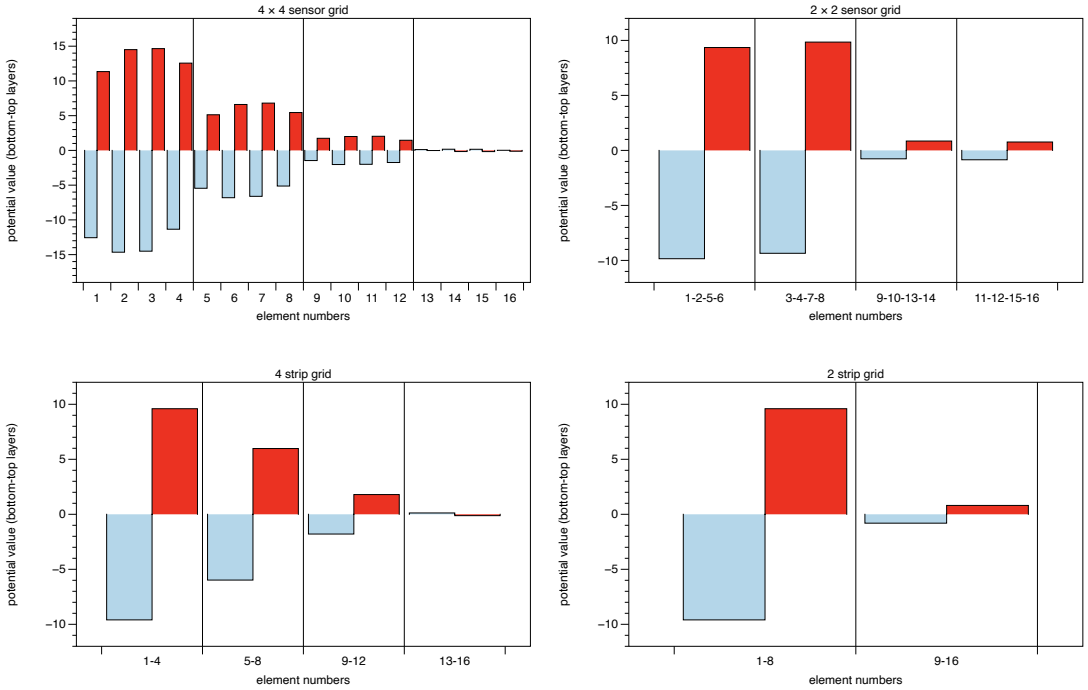

Figure 3: Clamped composite plate: effect of the segmentation of the piezoelectric patches in the sensor configuration for the four different segmentation of the patches.

(15 V) is obtained with the 4×4 grid; as the electrode size increases, the output voltage drops due to the potential redistribution over the equipotential patch.

3.2 Cylindrical shell panel

A cylindrical shell panel Fig. 4 (left), in the form of a quarter of a complete cylinder, is considered in this last numerical test in order to evaluate the shell FE approach. The problem is as follows [22]:

geometry cylindrical panel with $R_m = 200$ mm and $e = 2$ mm.

materials four-layer graphite-epoxy laminate $[0^\circ, 90^\circ]_S$ with a continuous PZT-4 actuator that is either bonded to the shell (at the inner surface or at the outer surface), or embedded at the center of the laminate. Each graphite-epoxy ply is ~~of~~ 0.375 mm thick, and the thickness of the PZT-4 actuator is 0.5 mm. The material properties are given in Tab. 1.

boundary conditions simply supported on the four edges; the PZT-4 layer is actuated with $\Delta\Phi = 200$ V.

mesh 4×15 elements (finer discretization along the circumferential direction).

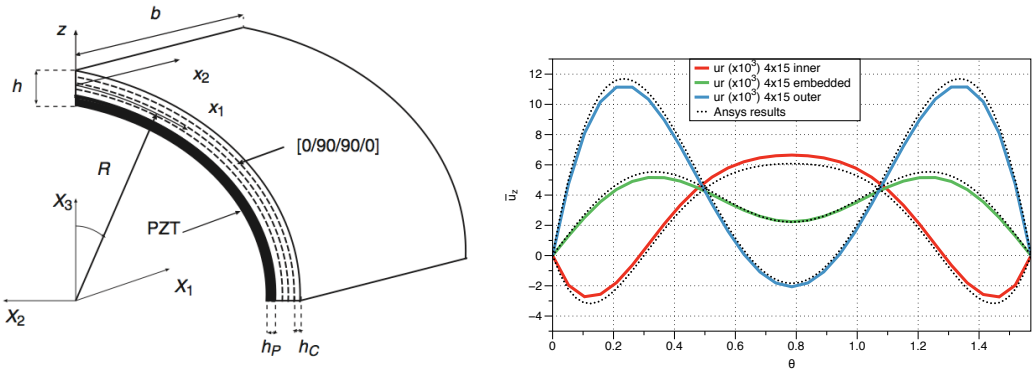

Figure 4: Simply supported cylindrical panel: description of the problem with $pz-$layer bonded at inner surface (left); distributions of the transverse displacement along the central line for the 3 locations of the piezoelectric layer (right).

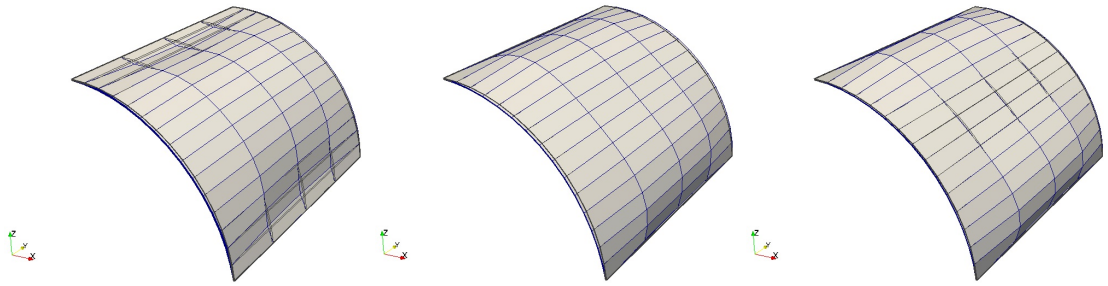

Figure 5: Deformed shapes of simply supported cylindrical panel for 3 different $pz-$layer locations: inner, embedded and outer , from left to right.

results and locations deformed shape and distributions of the transverse displacement along the center line of the cylindrical panel.

The distributions of the transverse displacement along the central curvilinear line of the cylindrical panel are presented in Fig. 4 (right). Present results are compared against those obtained by a full 3D simulation carried out with Ansys. The agreement is excellent, which confirms that this shell FE is able to capture the effect of the actuation with a very coarse mesh. In order to highlight the effect of the piezoelectric layer position in the structure, the three deformed shapes are given in Fig. 5. It can be seen that the shell panel curvature is strongly modified by the piezoelectric actuation and that very different shapes are obtained depending on the location of the actuator layer inside the stack.

4 Conclusion

This paper has presented a family of plate and shell FE for piezoelectric composite modelling. A high-order ESL kinematic model is considered that includes the sinus function for the in-plane displacements, a quadratic polynomial expansion for the transverse displacement and Zig-Zag functions for introducing slope discontinuities at layers' interfaces for both, the in-plane and the transverse displacements. The importance of this Zig-Zag terms was not presented in this short paper but it has been discussed in [4]. A LW cubic approximation is used for the electric potential in order to capture its non-linear distribution induced by the local bending of the piezoelectric layer; the elementary domain is considered as an equipotential surface (constant electric potential).

The element has been assessed through linear static case studies in both sensor and actuator configurations for laminated plates and shells. The role of electrode segmentation, i.e., the size of equipotential surfaces, on the electro-mechanical response has been also evaluated. The results are in good agreement for actuator and sensor configurations. This family of FE, using only 9, up to 12 mechanical dof per node, is very accurate, simple to use, without any numerical problem and could be used for a large range of thin to thick plate and shell problems involving piezoelectric patches or layers.

REFERENCES

[1] O. Polit, P. Vidal, M. D'Ottavio, Robust c^0 high-order plate finite element for thin to very thick structures: mechanical and thermo-mecanical analysis, International Journal for Numerical Methods in Engineering 90 (4) (2012) 429–451, dOI: 10.1002/nme.3328.

[2] H. Murakami, Laminated composite plate theory with improved in-plane response, J. App. Mech. 53 (1986) 661–666.

[3] J. Jiang, D. Li, A new finite element model for piezothermoelastic composite beam, J. Sound Vibr. 306 (2007) 849–864.

[4] O. Polit, M. D'Ottavio, P. Vidal, High-order plate finite elements for smart structure analysis, Composite Structures 151 (2016) 81–90.

[5] I. Chopra, Review of state of art of smart structures and integrated systems, AIAA Journal 40 (2002) 2145–2187.

[6] O. Polit, I. Bruant, Electric potential approximations for an eight node plate finite element, Computers and Structures 84 (22-23) (2006) 1480–1493.

[7] S. Gopinathan, V. Varadan, V. Varadan, A review and critique of theories for piezoelectric laminates, Smart Materials and Structures 9 (1) (2000) 24–48.

[8] R. Gibson, A review of recent research on mechanics of multifunctional composite materials and structures, Compos. Struct. 92 (2010) 2793–2810.

[9] E. Carrera, M. Boscolo, A. Robaldo, Hierarchic multilayered plate elements for coupled multifield problems of piezo- electric adaptive structures: formulation and numerical assessment, Archives of Computational Methods in Engineering 14 (4) (2007) 383–430.

[10] P. Vidal, M. D'Ottavio, M. Ben Thaïer, O. Polit, An efficient shell finite element for the static response of piezoelectric laminates, Journal of Intelligent Material Systems and Structures 22 (7) (2011) 671–690.

[11] S. B. Beheshti-Aval, M. Lezgy-Nazargah, P. Vidal, O. Polit, A refined sinus finite element model for the analysis of piezoelectric-laminated beams, Journal of Intelligent Material Systems and Structures 22 (3) (2011) 203–219.

[12] A. S. 176, IEEE Standard on Piezoelectricity, American National Standard Institute, 1987.

[13] H. Tiersen, Linear Piezoelectric Plate Vibrations, Plenum, New-York, 1969.

[14] M. Touratier, An efficient standard plate theory, Int. J. Eng. Sci. 29 (1991) 901–916.

[15] M. Ganapathi, B. P. Patel, P. Boisse, O. Polit, Flexural loss factors of sandwich and laminated composite beams using linear and nonlinear dynamic analysis, Composites Part B: Engineering 30 (3) (1999) 245–256.

[16] O. Polit, M. Touratier, A multilayered/sandwich triangular finite element applied to linear and non-linear analyses, Composite Structures 58 (1) (2002) 121–128.

[17] F. Dau, O. Polit, M. Touratier, C1 plate and shell finite elements for geometrically nonlinear analysis of multilayered structures, Computers and Structures 84 (19-20) (2006) 1264–1274.

[18] P. Vidal, O. Polit, A thermomechanical finite element for the analysis of rectangular laminated beams, Finite Elements in Analysis and Design 42 (10) (2006) 868–883.

[19] P. Vidal, O. Polit, A family of sinus finite elements for the analysis of rectangular laminated beams, Composite Structures 84 (1) (2008) 56–72.

[20] K. Lam, X. Q. Peng, G. R. Liu, J. N. Reddy, A finite-element model for piezoelectric composite laminates, Smart Mater. Struct. 6 (1997) 583–591.

[21] T. Liu, X. Sun, J. Zheng, L. Wang, Q. Liu, T. Q. Bui, Multi-patch isogeometric analysis for smart plates with distributed piezoelectric patches, Thin-Walled Structures 209 (2025) 112937.

[22] R. Kumar, B. Mishra, S. Jain, Static and dynamic analysis of smart cylindrical shell, Finite Elements in Analysis and Design 45 (2008) 13–24.